Memoirs of the Faculty of Science, Kyoto University, Series of Physics, Astrophysics, Geophysics and Chemistry, Vol. XXXVII, No. 2, Article 1, 1988

Pseudoscalar Meson Production in the Reaction $\pi^- p \to K^\pm K_s \pi^\mp n$ at 8.06 GeV/c

By

Ryuichi TAKASHIMA*

Department of Physics, Faculty of Science, Kyoto University, Kyoto 606, Japan

(*Received September 10, 1986*)

Abstract

The experimental study on the reaction

$$\pi^- p \to K^\pm K_s \pi^\mp n$$

at 8.06 GeV/c has been performed using a spectrometer at KEK. The number of pions incident upon the liquid hydrogen target amounted to 1.34×10^{11}. 4000 samples of the $K^\pm K_s \pi^\mp$ events have been collected. Two peaks at 1.28 GeV and 1.42 GeV are observed in the $K^\pm K_s \pi^\mp$ effective mass distribution. The masses and widths of these resonances are calculated to be D(1280): 1.280 ± 0.006 GeV(M), 15 ± 5 MeV(Γ) and E(1280): 1.424 ± 0.006 GeV(M), 35 ± 6 MeV(Γ). A partial wave analysis based on the isobar model has been performed to study the spin parity of D(1280) and E(1420). The result on D(1280) is $J^{PG}=1^{++}$ and on E(1420) is $J^{PG}=0^{-+}$ and different from the previous 1^{++} assignment. The decay mode of the E(1420) meson is found to be $\delta\pi$ with a little admixture of $K^*\overline{K}+\overline{K}^*K$.

1. Introduction

The color gauge theory has brought a great success to the quark model. The theory also predicts the bound states of gluons (glueball) by the direct gluon-gluon coupling. The spin, parity, mass and width of the glueball were estimated by some authors based on the lattice, bag and potential models of QCD.[1] The predicted mass is comparable to that of the ordinary meson.[1] The predicted J^{PC} are 0^{++}, 2^{++} and 0^{-+} for low mass states, where J, P and C are the spin, parity and charge conjugation quantum numbers, respectively. The verification of the glueball will give a strong support to the theory, especially to the non-aberian field property. Unfortunately the low mass states of glueballs have the same quantum numbers as $q\bar{q}$ states. So the identification of the glueball is very difficult. However, some guidelines to search glueballs were given by several authors. The first is the search for the state which can not be assigned to the $q\bar{q}$ multiplets of the quark model. The second is the search for the state produced in hard gluon process such as the radiative decay process of J/ψ.[2] The third is based on the flavor symmetry property that the glueball is SU(3) flavor singlet state.[3] The fourth is the narrowness of the state which is considered to be analogous to the OZI forbidden decay.[4] These last two properties of the glueball is useful to search the glueball.

* Now at the Department of Physics, Kyoto University of Education, Fushimi-ku, Kyoto.

Thus whole meson spectrum must be studied to account the possibility of existence of glueballs. The data accumulation of both favorable and unfavorable channels for the glueball production is very important to clarify the problem.

In hadronic reaction the E(1420) meson decaying into $K_sK^{\pm}\pi^{\mp}$ was observed in the $p\bar{p}$ annihilations at rest by Armenteros et al..[5] Subsequent analysis was performed by Baillon et al[6] for various charged states of the $K\bar{K}\pi$ system out of the $K\bar{K}3\pi$ state. The observation of the decay mode $K_sK_s\pi^0$ established its charge conjugation to be $C=+1$ and assigned to be $I^G=0^+$. The spin parity analysis resulted in the $J^P=0^-$ assignment.

The E(1420) meson has been also observed in the π^-p reaction[7] and in the $p\bar{p}$ annihilation at 0.7 and 0.76 GeV/c.[8,9] But these experiments preferred the $J^P=1^+$ assignment with less statistical significance.

Then in the the π^-p reaction at 4 GeV/c the production of the E(1420) mesons was observed by Dionisi et al. and assigned to the isoscalar of $J^{PC}=1^{++}$ nonet by the Dalitz plot analysis.[10]

Recently the Mark II group observed prominent peak near 1.4 GeV in the $K\bar{K}\pi$ mass distribution in the J/ψ radiative decay for the first time.[11] The decay branching ratio is shown to be comparable to that of the η' mesons and it was about 0.5% of whole J/ψ decay. The large branching ratio in the J/ψ radiative decay is one of the reason that this state is considered to be a glueball candidate. At the first stage of the analysis this state was considered to be the same state as the E(1420) meson. However, Ishikawa pointed out that the 1^{++} assignment is questionable[12] and Chanowitz claimed that this state is differnt from the E(1420) meson.[13] Crystalball group showed that the $J^{PC}=0^{-+}$ assignment was favorable and they named it the ι (1440) meson.[14] Crystalball group also showed that the branching ratio of the ι (1440) meson to $\eta\pi^+\pi^-$ was small.[15] This result conflicts with the fact that the ι (1440) meson seems to decay into $\delta\pi$ and that the δ (980) meson has a large branching ratio decaying into $\eta\pi$. This fact has been considered to be very puzzling.

The radiative decay process was further studied by the MARK III group with high statistics.[16] The Berman-Jacob technique which did not contain the assumption on the two body decay properties of the ι (1440) meson was used to assign the spin and parity. The result showed an agreement with the previous $J^P=0^-$ assignment.

On the other hand the E(1420) meson was observed with better statistics in the central region production in the pp and π^+p reactions by the Omega spectrometer at CERN and the E(1420) meson was assigned again to 1^{++} by Dalitz plot analysis.[17] However, in the recent high statistics π^-p charge exchange experiment at 8 GeV/c, a prominent enhancement near 1.42 GeV was observed by the multiparticle spectrometer at BNL and assigned to $J^{PC}=0^{-+}$ by Zemach amplitude analysis.[18]

The $\pi^-p \to \eta\pi^+\pi^- n$ reaction was studied for the first time by Stanton et al. at 8.45 GeV/c and they found the pseudoscalar resonance at 1.27 GeV by the partial wave analysis (PWA).[19] The same process at 8.06 GeV/c was also studied by the charged and gamma spectrometer at KEK.[20] By the partial wave analysis based on the isobar model the pseudoscalar mesons around 1.27 GeV and 1.42 GeV in the $\delta\pi$ wave were observed. The $\delta\pi$ and $\varepsilon\eta$ waves interfere destructively in the mass region of 1.42 GeV.

This fact explains the suppression of the enhancement of 1.42 GeV in the $\eta\pi^+\pi^-$ mass distribution.[20]

The status among the E(1420) meson and the ι(1440) meson is very much confusing as briefly summarized above. The spin-parity assignment of the E(1420) meson is still ambiguous. The problem related to the decay mode of the ι(1440) meson is not clearly understood. In addition to these whether the E(1420) meson and the ι(1440) meson are the same or different states is an open problem. These problem to be solved deeply related to whether the ι(1440) meson could be a glueball.

We studied the reaction

$$\pi^- p \longrightarrow K^{\pm} K_s \pi^{\mp} + n$$
$$\qquad\qquad\quad \hookrightarrow \pi^+\pi^-,$$

with the same spectrometer as that was used to study the $\eta\pi^+\pi^-$ state in the $\pi^- p$ charge exchange reaction at KEK.[20,21] In this experiment, the $K^{\pm}$, K_s and $\pi^{\mp}$ mesons emerging in the forward angles have been detected by the magnet spectrometer to identify the above reaction. This hadronic forward production proceeds mainly through the peripheral reaction, and the dominant state which is produced by the peripheral production has quarkonium component. Therefore, the production of the glueball is expected to be suppressed in this experiment.

2. Experimental Apparatus

Pions were produced in a Cu target of 10 mmϕ×60 mm irradiated with typically 8 ×10^{11} protons per burst accelerated by the 12 GeV proton synchrotron at National Laboratory of High Energy Physics (KEK). The synchrotron was operated with a repetition rate of 1/2.5 per second. Then the pions were analyzed their momentum through the $\pi-1$ beam line consisting of two superconducting bending magnets and four quadrupole magnets, and focused onto a liquid hydrogen target. The typical intensity of the 8.06 GeV/c pion beam was 8×10^4 per burst with a momentum bite of 1.2%. The beam size at the target was 30 mm in diameter. The liquid hydrogen target had a cylindrical shape of 21 cm in length and 5 cm in diameter.

The particles emerging from the hydrogen target were detected by the charged and gamma spectrometer as shown in Fig. 1. The performance of the detector system was reported already.[21] The charged particles emitted in the forward direction were analyzed by the window frame magnet with a large aperture which is named BENKEI and has the field integral of 12 kgauss-m. The effective volume is 1.0 (height)×1.5 (width)×2.2 (length) m^3. The magnetic field was measured at 8000 points in the one eighth of the effective volume assuming the field symmetry. The trajectries of the charged particles were recorded by four sets of stacked wire chambers. In each set of the stacked chambers, one multi-wire proportional chamber (MWPC) and a pair of drift chambers(DC) were provided for the measurment of vertical or horizontal position. Therefore, each set of stacked chambers consists of two MWPC's and four DC's. A pair of DC's are staggered to resolve the left and right ambiguity. Among the 16 DC planes, five planes are of the charge division type. Thus, the informations from the two

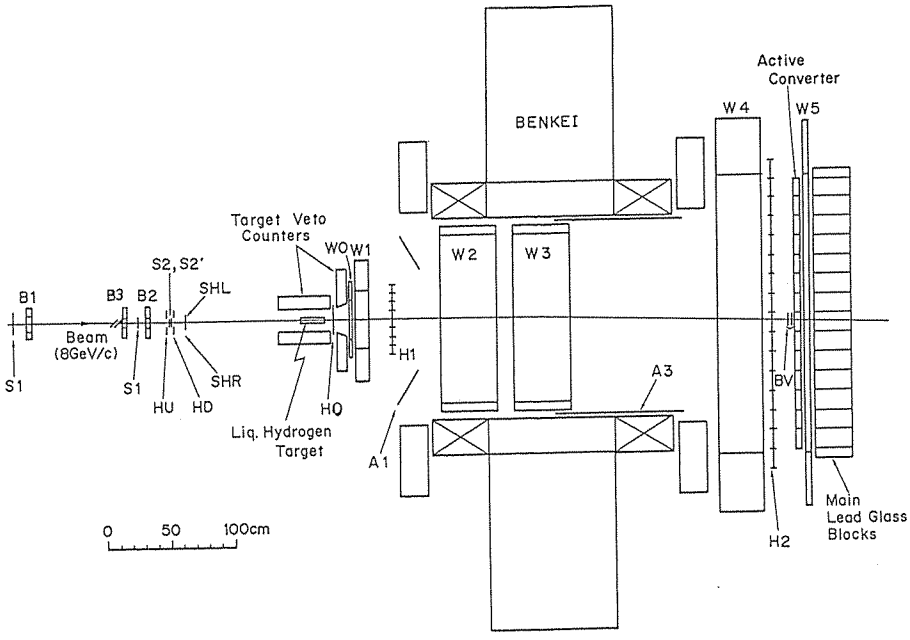

Figure 1 Experimental layout.

dimensional readout are crucial in order to reconstruct the complicated pattern of four prong event. The counter hodoscope(H2) is used to measure the time of flight of particles to distinguish kaons and pions. The target is surrounded by twenty-five veto counters except in the forward direction to reject unwanted events. These veto counters consisting of scintillator and lead sheets are sensitive to not only charged particles but also gamma rays. At the latter stage of the experiment, a beam chambers (B3) and a MWPC (W0) were added to improve the measuremnt of trajectries of the incident beam and the emitted multiple charged particles, respectively. The TOF counters were also changed from the counters of 1 cm thick made of NE110 to the ones of 3 cm made of KYOWA SCSN type.[22] This replacement improved the time resolution of the TOF system and made it possible to distinguish the charged kaon and pion. In the early stage of the experiment, discriminators of constant fraction type were used for the TOF measurement, however, at the middle of running, these discriminators were replaced by leading edge discriminators and pulse heights were recorded by ADC's. The informations of pulse heights were used in the off line analysis to correct the time deviation due to the pulse heights.[23]

The trigger signals for the electronic data acquisition system were provided in the following two levels. At first the beam signals were generated by using the series of scintillation counters of S1, S1', S2, and S2' placed upstream of the liquid hydrogen target. This signal was also vetoed by the hole counters of HU, HD, SHL and SHR. As was mentioned, in this experiment only four prong events were measured, so that at least two hits were required for the upstream hodoscope (H1) and at least four hits for the downstream one (H2). No hit at the target veto counters (TV) and in the

acceptance of the veto counters (A1, 2, 3) were required. The trigger signals which satisfied above requirement and in coincidence with the beam signals were generated as the first level trigger. The logic of the first level triggers can be expresed as follows;

$$S1*S1'*S2*S2'*H0*(H1>1)*(H2>3)*\overline{(SHL+SHR+HU+HD+A1+A2+A3+BV1*BV2+TV)}.$$

The signals from all chambers were latched and the analog to digital convertors were triggered by the first level triggers. The second level triggers were generated by a fast selective trigger logic module. This CAMAC module contains sixteen random access memories (RAM) of 256 bits whose 16 address lines are not coded and act like a programmable coincidence module of 64×64. In this selective trigger logic the event which had at least three hits for the MWPC at the center of magnetic field were selected within about one μ second. This trigger mode is called as "4C trigger".

The data acquisition system in our experiment was unique one using a system of encoders and a buffer memory.[24] The data latched in the CAMAC modules were transfered to the eight buffer memories of 16 K bytes. The encoder and buffer memory system enables us to handle several tens of events per beam spill of 400 m seconds with very small dead time. The data transfered in the buffer memory during the beam spill were sent to a PDP11/34 minicomputer interfaced by a ordinary branch driver during the beam off time.

3. Data Analysis

About 1200 hours have been consumed on the data taking run with the 4C trigger mode. Total 1.34×10^{11} pions were icident on the liquid hydrogen target and total numbers of triggers amounted to be 4×10^{6}. The off line analysis of the data has been performed on the KEK FACOM-HITAC M200H central computer system. The spatial resolution of the drift chambers was measured as the deviation of the hit point from the fitted point and found to be 800 μm (FWHM). The spatial resolution of the charge division DC's along the wire direction obtained by the charge division method was found to be about 2% (FWHM) of the wire length. The resolution of the time of flight measurement between the S2 and H2 counters was 500 psec(FWHM).

In order to select the event of the $K^{\pm}\pi^{\mp}K_s(\pi^+\pi^-)n$ final state, the trajectries of four charged particles were reconstructed in vertical and horizontal planes separately. The trajectries are almost straight in the vertical plane because the major component of the magnetic field is vertical. Therefore, the trajectries in the vertical plane were reconstructed for all four prongs successively at first. Then the reconstruction of trajectries in the horizontal plane was performed. However, the reconstruction in the horizontal plane was rather complicated, because the trajectries are bent by magnetic field and crossing each other. At first four straight trajectries in front of the magnetic field were reconstructed from the hits on the W0, W1 and W2 chambers. The informations from the two dimensional detectors, such as the charge division DC's and TOF counters, used in the vertical track reconstruction were very usefull. Finally the

tracks were fitted by the spline method[25] and momentum vectors were obtained.

The total momentum distribution in Fig. 2 shows the clear peak around the beam momentum of 8 GeV/c, since the cross section is large in the forward direction.

From the four charged particles events thus reconstructed, only the events which are totaly neutral were selected. In order to tag the K_s mesons, the vertex topology of the vee event was employed. Among the two combinations of unlike sign particles we selected, the one whose sum of two minimum distances between two tracks at the target region was shorter was selected. With this selection the clear K_s peak was observed in the 2π mass distribution while the other combination does not give the K_s peak as shown in Fig. 3. In order to assign which piar to be K_s, the medium point of the lines of the minimum distance between the trajectries of the pair of unlike sign particles was regarded as a vertex point. Then the distance between two vertex points was required to be more than 1 cm. Among the two vertex points the one which lied downstream than the other was regarded as the decay point of K_s. The decay point was also required to be less than 40 cm from the target center. Furthermore the

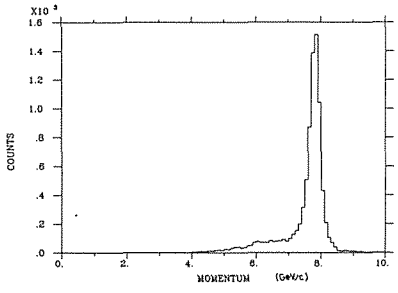

Figure 2 Total momentum distribution without the missing mass cut.

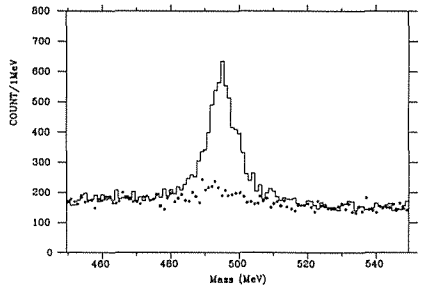

Figure 3 Effective mass of the two particles of unlike sign. Within two combinations the one which gave the shorter sum of minimum distances of the two lines was selected as the events. The distribution of the events which give longer sum is plotted by • .

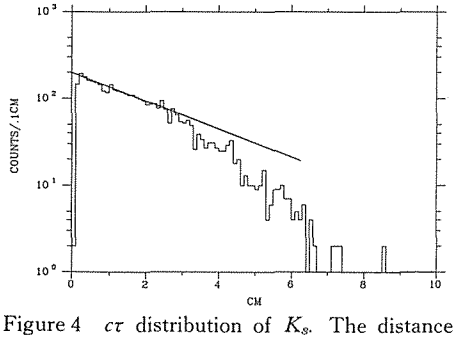

Figure 4 $c\tau$ distribution of K_s. The distance between two vertex points was divided by $\beta\gamma$ of K_s calculated from the measured momentum.

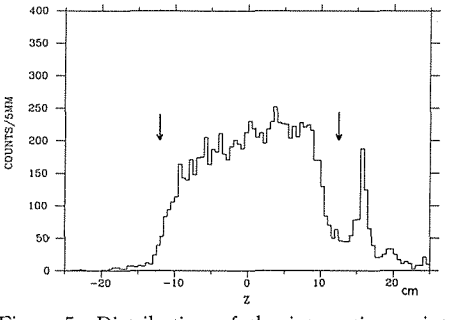

Figure 5 Distribution of the interaction point along the z-axis.

invariant mass of the pair of particles from the decay point was required to lie in the region between 490 and 502 MeV. The $c\tau$ distribution of thus selected K_s is shown in Fig. 4, where c and τ are the light velocity and the proper decay time, respectively. The distribution shows the linear exponential decay and a good agreement with the expected distribution. The deviation at the longer life time is due to the shape of the acceptance.

The other vertex point, upstream one, was regarded as the reaction point of the $\pi^- p \to K^{\pm} K_s \pi^{\mp}$ event. The distribution of the reaction points along the beam(z) axis is shown in Fig. 5. The peak at the downstream of the target is a background due to the trigger counter(H0). The target cut is indicated in the figure.

The invariant mass of the two particles from the reaction point also shows the prominent K_s peak assuming that both particles were pions at this stage. This peak is due to K_s produced in the $\pi^- p \to K_s K_s n$ reaction. The event that the effective mass of the two particles lays in the region between 490 and 502 MeV was cut off to eliminate this $K_s K_s n$ events.

At the next stage the particles of two charged tracks from the reaction point were identified as $K^{\pm}$ or $\pi^{\mp}$. Fig. 6 shows the scatter plot of momentum versus the mass of these tracks which were calculated from the TOF measurement between S2 and H2. As shown in the figure, the identification at higher momentum region was rather difficult. In order to assign the particle spieces, the following variable R was calculated.

$$R = (T_1 - T_\pi)^2 + (T_2 - T_K)^2 ,$$

where T_1 and T_2 are the time of flight of the two particles, and T_π and T_K were the time which is calculated by assuming that the particle are pion and kaon, respectively. In Fig. 7, the R distribution for both favorable and opposite assignments are shown together with the cut.

Using the kinematical valuables of all four particles thus assigned, the missing mass was calculated. The missing mass squared distribution is shown in Fig. 8. A single clear peak corresponding to the neutrons and small background at higher mass

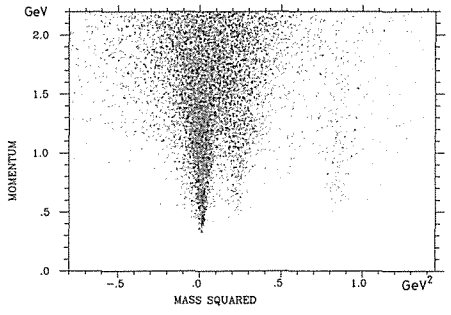

Figure 6 Mass squared calculated by the TOF measurement versus that from the measured momentum.

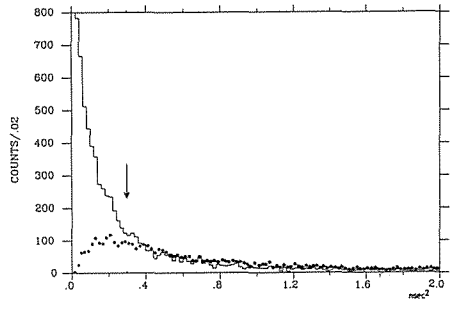

Figure 7 Sum of the time deviation squared of the TOF measurement from the time calculated by using momentum and the assumed masses. The favorable assignment is plotted in histogram and the unfavorable one is plotted by •.

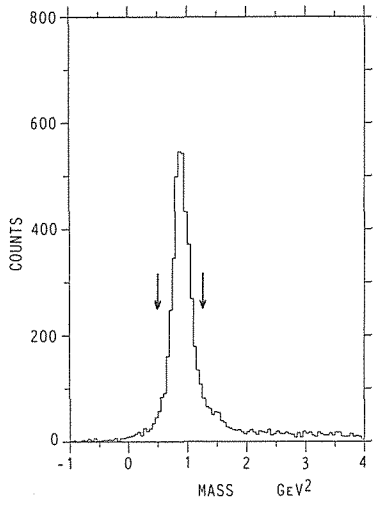

Figure 8 Missing mass squared distribution.

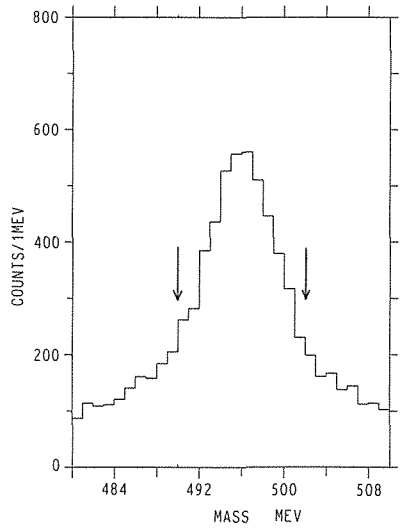

Figure 9 Effective mass distribution of $\pi^+\pi^-$ after all cuts.

region are seen. The effective mass of the recoil neutron whose momentum was obtained from the kinematical calculation and one of mesons was also calculated. This effective mass distribution shows no structure which is caused by nucleon resonance or hyperon. Thus, the $\pi^- p \to K^\pm K_s \pi^\mp n$ reaction is clearly confirmed.

The effective mass distribution of $\pi^+\pi^-$ assigned as K_s is shown in Fig. 9. It is seen that the background contribution from 4π production is rather small. The mass resolution of K_s was 9 MeV(FWHM). It agrees with the value of the Monte Carlo calculation with the DC resolution of 800 μm. Finally 4000 events of $K^\pm K_s \pi^\mp$ remained for both charge states.

The $K^\pm K_s \pi^\mp$ mass distribution of the finally selected events is shown in Fig. 10. The prominent peak is seen around 1.28 and 1.42 GeV. The distribution was fitted by the Breit Wigner resonance formula and background with MINUIT program and is seen in Fig. 11. The fitted masses and widths are listed in Table 1. The mass resolution of the spectrometer was simulated by the Monte Carlo method and found to be 9 MeV(FWHM) in this mass region.

In Fig. 12a the so-called Chew-Low plot is shown. The mass distribution of the event whose momentum transfer is greater than 0.25 GeV² is shown in Fig. 12b. Two peaks are enhanced considerably in this high momentum transfer region.

The effective mass distribution of $K_s K^\pm$ is shown in Fig. 13a. The sharp rise at the threshold of the effective mass indicates that there exists the considerable amount of δ (980) which is the iso-vector state of the scalar meson nonet. In the effective mass distribution of $K\pi$ there is a prominent peak of K^* (890) as shown in both Fig. 13b and 13c. These features indicate that the considerable amount of the final $K\bar{K}\pi$ states were produced through the intermediate states of $\delta\pi$ or K^*K.

The contribution of the $\delta\pi$ or K^*K state to the intermediate state was studied applying the cuts. When the events which the $K_s K^\pm$ mass lie in the region less than

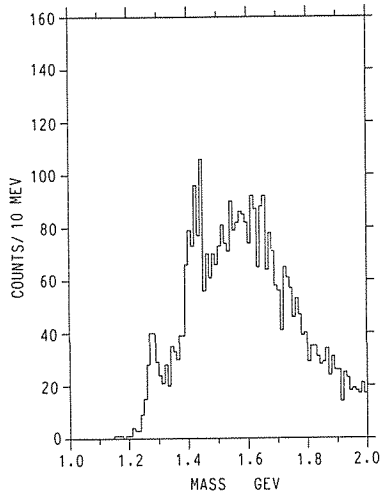

Figure 10 $K_sK^{\pm}\pi^{\mp}$ effective mass distribution.

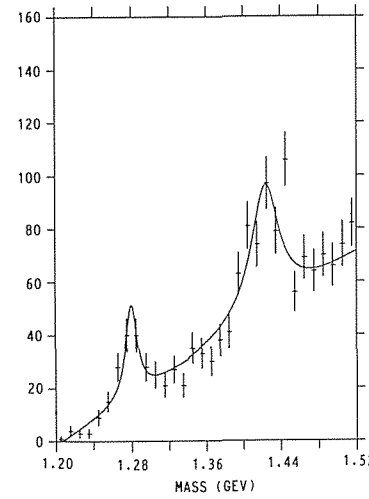

Figure 11 $K_sK^{\pm}\pi^{\mp}$ effective mass distribution and a fitting by the Breit Wigner function.

Table 1 Fitted mass and width with the Breit Wigner function

Mass(D)	1.280±0.006Gev
Γ(D)	15± 5 Mev
Mass(E)	1.424±0.006Gev
Γ(E)	35± 6 Mev

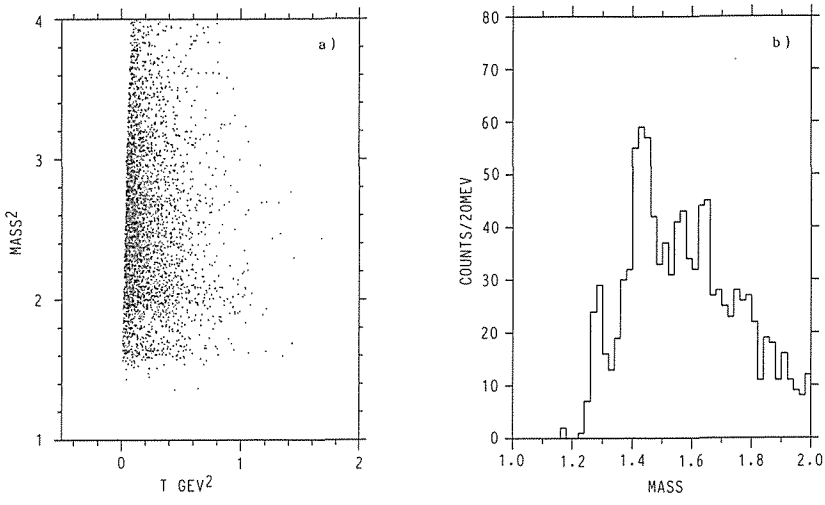

Figure 12a Chew-Low plot for the $K_sK^{\pm}\pi^{\mp}$ state.
12b $K_sK^{\pm}\pi^{\mp}$ effective mass distribution with $t'>0.25$ GeV^2.

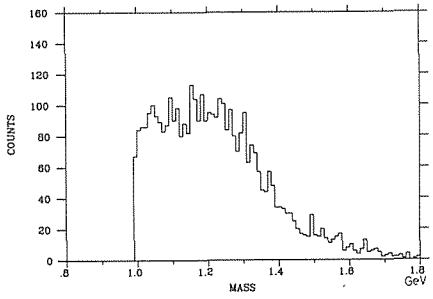

Figure 13a Effective mass distribution of the $K_sK^{\pm}$ state.

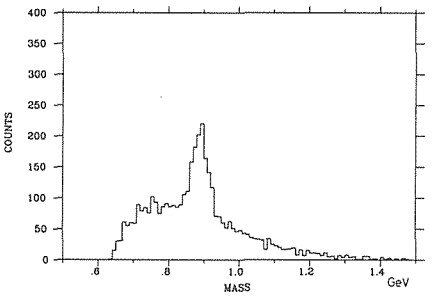

13b Effective mass distribution of the $\pi^{\mp}K^{\pm}$ state.

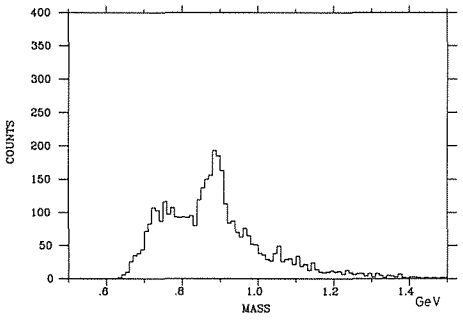

13c Effective mass distribution of the $\pi^{\mp}K^{\pm}$ state.

1.04 GeV were selected, still the two peaks at 1.28 GeV and 1.42 GeV in the $KK_s\pi$ distribution remain as shown in Fig. 14a. The number of the events under the peak at 1.28 GeV is the same as that of the all events, while the number of events under the peak at 1.42 GeV is reduced to be a half of the total events. This indicates that the state at 1.28 GeV mostly decays through the $\delta\pi$ mode and about a half of the state at 1.42 GeV decays through the $\delta\pi$ mode. The $KK_s\pi$ mass distribution which includes only K^*, that is to say, the $K\pi$ effective mass lies between 0.84 GeV and 0.93 GeV are shown in Fig. 14b and 14c. Both distributions include a large fraction of events in the

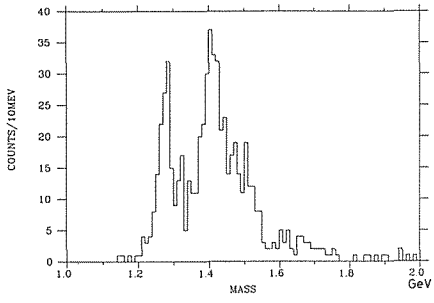

Figure 14a Effective mass distribution of the $K_sK^{\pm}\pi^{\mp}$ state.
($m_{K_sK}\pm<1.04$ GeV)

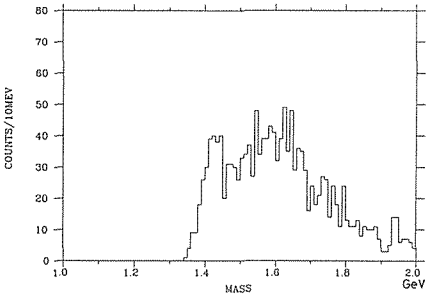

14b Effective mass distribution of the $K_sK^{\pm}\pi^{\mp}$ state.
($0.84<m_{\pi^{\mp}K_s}<0.93$ GeV)

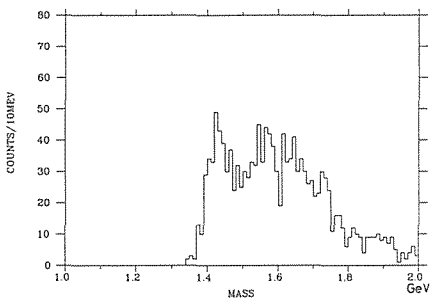

14c Effective mass distribution of the $K_sK^{\pm}\pi^{\mp}$ state.
($0.84 < m_{\pi^{\pm}K^{\pm}} < 0.93$ GeV).

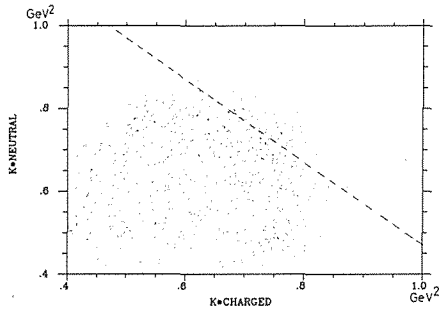

Figure 15 Dalitz Plot ($1.39 < m_{K\bar{K}\pi} < 1.45$ GeV).

high mass region and show the dominat production of the K^*K intermediate state.

The Dalitz plot in the mass region of $K\overline{K}\pi$ from 1.40 GeV to 1.44 GeV is shown in Fig. 15. The line shows the effective mass of $K\overline{K}$ to be equal to 1.05 GeV. It is seen that there exists the K^* band and also a considerable amount of events around the δ line. The 1.42 GeV peak seems to decay comparably through K^*K and $\delta\pi$. As shown in Fig. 14a, b and c, the 1.42 GeV peak remains after the simple K^* and δ cuts. In order to study two peaks in more details, it is necessary to do more systematic analysis in stead of the simple kinematical analysis.

4. Isobar Model Analysis

An isobar model analysis[26] has been performed to determine the quantum numbers of mesons and the decay process, In this analysis, it is assumed that the $\pi^- p$ interaction produces a meson (X) and a neutron, then the produced meson decays into an isobar and a bachelor meson, and finally an isobar into dimeson as shown in Fig. 16. The kinematical variables to describe the production of the X meson are W and t. where W and t are the invariant mass of the meson and the momentum transfer squared, respectively. The five independent kinematical variables, α_j, β_j, γ_j, ω_j and θ_j are sufficient to describe the decay into three mesons in the Gottfried-Jackson frame by the conservation of four momenta. The variables, α_j, β_j and γ_j, are the Euler angles of the three meson decay frame with respect to the Gottfried-Jackson frame as shown in Fig. 17. The both frames are the rest frame of three mesons. The variables, ω_j and θ_j, are the isobar mass and the decay angle of the isobar, respectively. θ_j is defined as an angle between the direction of the isobar and the decay particle of k in the frame of isobar at rest. The subscripts of j, k and l denote the three outgoing particles. In our case, these can be any cyclic permutation of $K^{\pm}$, K_s and $\pi^{\mp}$. It should be noted that the isobar is always composed of the meson of k and l. The isobar can decay into any one of the $K^{\pm}K_s$, $\pi^{\mp}K_s$ and $\pi^{\mp}K^{\pm}$ in this case. The subscript j indicates all quantities pertaining the isobar.

The state of the produced meson X will be characterized by a wave function ψ in the form of

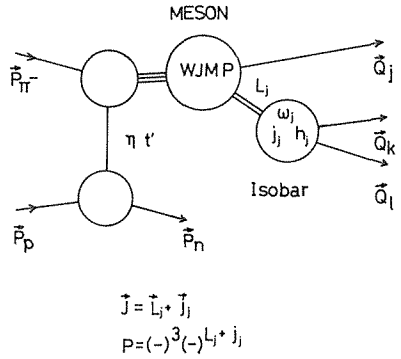

Figure 16 The isobar model. The subscripts of J, k and l denote the three outgoing particles. In our case, those are any cyclic permutation of $K^{\pm}$, K_s and $\pi^{\mp}$. It should be noted that the isobaris always composed of mesons of k and l. The subscript j denotes all quantities pertaining the isobar.

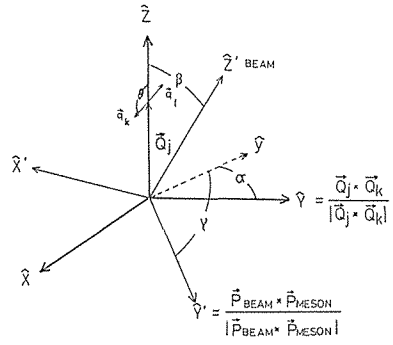

Figure 17 Coordinate systems. The (x, y, z) system represents the three particles decay frame and the (x', y', z') system represents the Gottfried Jackson frame.

$$\psi = \sum_c P^c(W, t')|c> \ , \qquad \text{with} \qquad t' = |t - t_{\min}| \ ,$$

where $P^c(W, t')$ is the production amplitude. In this expression, c denotes a set of quantum numbers (J, M, L_j, j_j), where J and M are the total spin of the (j, k, l) system and the z-component of J in the production frame, respectively. L_j is the relative angular momentum between the isobar and the bachelor meson, while j_j is the spin of the isobar. t is the momentum transfer squared and $t_{\min}$ is the minimum value of $-t$.

The transition matrix elements of X into the three particle state are written for the decay configuration shown in Fig. 17. Note that the momentum vector of the isobar has the opposite direction on the z-axis of the three particle decay frame.

$$G_c = (W\omega_j/\pi^2 Q_j q_k)^{1/2} [(2L_j+1)(2J_j+1)]^{1/2}$$
$$\times \sum_{hj} D^J_{-h_j M}(\alpha_j, \beta_j, \gamma_j)\, C(L_j, j_j, J|0, -h_j)\, d^{j_j}_{-h_j 0}(\theta_j)\, T_{JL_j}(W)\, F_j(\omega_j) \ ,$$

where q_k and h_j are the momentum of the meson (k) in the center of mass system of the isobar and the helicity of the isobar, respectively. Q_j denotes the momentum of the bachelor meson in the G-J frame. $D^j_{m'm}$ is the rotation matrix of $(2J+1)$ dimensional representation of the rotation group. d is so called d function. $C(j_1, j_2, J|m_1, m_2)$ is the Clebsch-Gordan coefficient.

Using the Watson theorem and the relativistic Breit-Wigner form, the reduced matrix elements of the two body decay $T_{JL_j}(W)$ and $F_j(\omega_j)$ are written as

$$T_{JL_j}(W) = (Q_j/4W)^{1/2}(B_L(Q_j))^{1/2}\, Z(W) \ ,$$

$$F_j(\omega_j) = (q_k/4\omega_j)^{1/2}(\omega_j/q^{1+1})\, BW(\omega_j) \ ,$$

with

$$BW(\omega_j) = \frac{\omega_j \Gamma(\omega_j)}{(\omega_0 - \omega_j)^2 - i\omega_0 \Gamma(\omega_j)},$$

and

$$\Gamma(\omega_j) = \Gamma_0 \frac{p_K(\omega_j)\, B_j(q_K(\omega_j))}{p_K(\omega_0)\, B_j(q_K(\omega_0))},$$

where $B_{Lj}(Q_j)$ is the standard Blatt-Weiskopf barrier factor with the spin of L_j.[27] Γ is the width parameter. The reduced matrix element $Z(W)$ can be considered as a constant by taking the small mass bin of the three meson system.

For the case in which the isobar is the δ meson ($\delta \to K\overline{K}$), the parameters are chosen to be $\omega_0 = 0.98$ GeV and $\Gamma_0 = 0.050$ GeV. For the case of the isobar ($K^* \to K\pi$), the parameters are $\omega_0 = 0.89$ GeV and $\Gamma_0 = 0.050$ GeV.

The decay matrix element is not decomposed into the isospin component, because the isospin symmetry is not sufficient enough to discribe the $K\overline{K}\pi$ state. The symmetry based on the strangeness must be taken into the analysis. In this case, G-transformation is symmetric. The wave functions of $K^*\overline{K} \pm \overline{K}^*K$ represent the eigen state of G-parity of positive and negative, respectively. Therefore, by observing the interference between the $K^*\overline{K}$ and $\overline{K}^*K$ waves, the G-parity can be determined.

The wave fuctions can be written by the eigen state of the reflection parity operator which is introduced by T. D. Hansen et al.[28] and reflect the state with respect to the x-z production plane in this case. The wave functions with the different eigen value do not interfere, so that the correlation matrix can be simplified. This reflection is performed by taking the real part of the D function for plus eigen value ($\eta = +1$) and imaginary for negative eigen value. ($\eta = -1$)

Finally, the yield at each value of mass (W) and t' is expressed as,

$$F(W, t') = \int \sum_{\eta} \left| \sum_{c} P^c(W, t')\, G_c(\vec{y}) \right|^2 \mathrm{d}\vec{y},$$

where $\vec{y}$ represents the five kinematical variables. The present spectrometer has a finite acceptance of $A(W, \vec{y}, t')$. The acceptance $A(W, \vec{y}, t')$ was calculated by the Monte-Carlo method. Therefore, the actual yield F_{nor} can be written as

$$F_{\mathrm{nor}}(W, t') = \int \sum_{\eta} \left| \sum_{c} P^c G_c(\vec{y}) \right|^2 A(W, \vec{y}, t')\, \mathrm{d}\vec{y}$$

$$= \sum_{\eta} \sum_{c1} \sum_{c2} P^{c1}\, P^{c2} X_{c1c2},$$

$$\text{where } X_{c1c2} = \int G_{c1} G_{c2}\, A(W, \vec{y}, t')\, \mathrm{d}\vec{y}.$$

To obtain the production amplitudes, $P^c(W, t')$, the extended maximum likelihood method[29] was employed. The following logalismic likelihood function is maximized in the each mass and t' bin.

$$\ln L(W, t') = \sum_{k}^{event} \{ \ln [\sum_{\eta} | \sum_{c} P^c(w, t') G_c(\vec{y}_k) |^2]$$

$$- \ln [\sum_{\eta} \sum_{c1} \sum_{c2} P^{c1}(W, t')\, P^{c2}(W, t') X_{c1c2}] \},$$

where $G_c(\vec{y}_k)$ denotes the matrix element calculated for the k-th event.

Since the distribution of five kinematical variables for the $K^+K_s\pi^-$ and $K^-K_s\pi^+$ states were carefully tested and found to be similar for both charge states, the data of both charge states were combined in the partial wave analysis. The analysis should be performed for each t' bin. However, due to the limited statistics of the data, the value of t' was fixed to 0.1 GeV^2 in this Monte-Carlo calculation, and the events of which t' is less than 1.2 GeV^2 were included in the analysis. The events were sorted in the $K\overline{K}\pi$ mass (W) of 20 MeV bin. The solution was searched for each mass bin independently.

The automated solution searching procedure[30] was used incorporating with the modified version of OPTIME[31] fitting package. The input waves which were tested in the analysis are listed in Table 2. The waves are described by the set of quantum numbers ($JPGI_sLM\eta$). J, P and G are the total spin, parity and G-parity of the produced meson, respectively. I_s, L, M and η denote the isobar, the relative angular momentum between isobar and bachelor meson, the magnetic quantum number of the meson at production frame, and the exchange naturality, respectively. The parity P is determined by the parities of the isobar and the bachelor meson and L.

For the isobar which decays into the $K\overline{K}$ system, the states of $I^G(J^P)=1^-(0^+)$ and $1^+(1^-)$ are allowed because of the symmetrical property of the $K\overline{K}$ system. But only the δ meson ($1^-(0^+)$) satisfies this condition in this mass region. By the conservation of G-parity, the states of the positive charge conjugation ($C=+1$) are allowed to decay into $\delta\pi$. Therefore, among the mesons of interest the isoscalar meson of $J^{PC}=0^{-+}$ and 1^{++} are allowed, while the 1^{+-} mesons are forbidden to decay into $\delta\pi$.

The $K^*(890)$ meson is also a candidate of the isobar which should be considered in this mass region. The K^*K waves contain both G-parity states.

Concerning to the relative angular momentum between the isobar and bachelor meson, only the S and P waves were included in the analysis.

Table 2 List of the fitted waves

Tested waves $JPGI_sBLM\eta$	Fitted waves $JPGI_sBLM\eta$	Tested waves $JPGI_sBLM\eta$	Fitted waves $JPGI_sBLM\eta$
$0-+\delta\pi S0+$	$0-+\delta\pi S0+$	$1+-K^*KD0+$	.....
$1++\delta\pi P0+$	$1++\delta\pi P0+$	$1++K^*KD1+$	.....
$1++\delta\pi P1+$	$1++\delta\pi P1+$	$1+-K^*KD1+$	.....
$0-+K^*KP0+$	$0-+K^*KP0+$	$1++\delta\pi P1-$	$1++\delta\pi P1-$
$0--K^*KP0+$	.....	$1++K^*KS1-$	.....
$1++K^*KS0+$	$1++K^*KS0+$	$1+-K^*KS1-$	.....
$1+-K^*KS0+$	$1+-K^*KS0+$	$1-+K^*KP0-$	$1-+K^*KP0-$
$1++K^*KS1+$	.....	$1--K^*KP0-$	$1--K^*KP0-$
$1+-K^*KS1+$	.....	$1-+K^*KP1-$	.....
$1-+K^*KP1+$	.....	$1--K^*KP1-$	.....
$1--K^*KP1+$	.....	$1++K^*KD1-$	.....
$1++K^*KD0+$	.....	$1+-K^*KD1-$	.....

5. Results of the Fitting

The solutions were searched for various combination of initial values in each $K\bar{K}\pi$ effective mass bin. The set of tested waves and the waves which are found to be sufficient to describe the data are listed in Table. 2.

The distribution of five kinematical variables of the data were compared with the Monte Carlo event using the fitted amplitude of the above mentioned waves. The solutions reproduce the measured distributions of five kinematical variables (ω, θ, α, β, γ), as is seen in Fig. 18.

The intensities of the significant waves corrected with the acceptance are shown in Fig. 19.a-d. The wave of $J=1$, $P=+$, $G=+$, $I_s=\delta$ (Isobar), $B=\pi$ (bachelor), $L=P$, $M=0$ and $\eta=+(1++\delta\pi P0+)$ has a peak at 1.28 GeV which corresponds to the D (1280) meson. There is no significant peak at 1.42 GeV in this wave, while the $0-+\delta\pi S0+$ wave has a large amplitude at 1/42 GeV. The $0-+K^*KP0+$ wave has the broad peak at 1.52 GeV. The $1--K^*KP0-$ wave increases its amplitude as the mass goes up to the 1.6 GeV region. The other waves do not show the stable behavior. For instance, the $1+-K^*S0+$ and $1++K^*S0+$ waves are interesting to search for the missing isoscalar of $J^{PC}=1^{+-}$ and 1^{++} nonets, however these waves show no peaks. The phase motion is also unable to be confirmed for these waves.

Since the 1.28 GeV peak in the effective mass distribution is mainly due to the $1++\delta\pi$ and a small contribution from the $0-+\delta\pi$ waves, this peak corresponds to the production of the D (1280) meson and it is also consistent with the result obtained from the $\eta\pi\pi$ production data reported by Ando et al.[20]

The peak observed at 1.42 GeV in the effective mass distribution of the $K\bar{K}$ system coinsides with the peak in the $0-+\delta\pi S0+$ wave. The spin parity of 0^{-+} can be assigned to the E (1420) meson. This assignment agrees with that by Chung et al.[18] but disagrees with that by Dionisi et al.[10] Chung et al. reported that the $0-+K^*K$ wave has a large contribution in this mass. This result is also consistent with the observation of the pseudoscalar resonance in the $\eta\pi\pi$ final state at 1.42 GeV[20], because the δ (980) meson can decay into the $\eta\pi$ system.

Thus, present assignment of the spin-parity and the decay mode are the same as the ι (1440) meson found in J/ψ radiative decay. However, the present result on mass and width of the E(1420) meson(35 MeV) are different and smaller than those of the ι (1440) meson (76 MeV).

There is a broad structure above the 1.42 GeV peak in the effective mass distribution. The $0-+K^*K$ wave which has a peak around 1.52 GeV has a rather large amplitude. The $0-+K^*K$ wave and the $0-+\delta\pi$ wave are the complementary in this analysis. For instance, when the $0-+K^*K$ wave is set to be zero, the $0-+\delta\pi$ wave must be large. However, in this region, the K^*K wave dominates over the $\delta\pi$ wave according to the kinematical analysis as mentioned in the previous section. The result of the partial wave analysis that the $0-+K^*K$ wave dominates above 1.42 GeV agrees with the kinematical one. However, it is not clear whether the enhancement around 1.52 GeV is a resonance which corresponds to a isoscalar of $J^{PC}=0^{-+}$ nonet or not, because the present analysis dose not include higher partial waves and our invariant

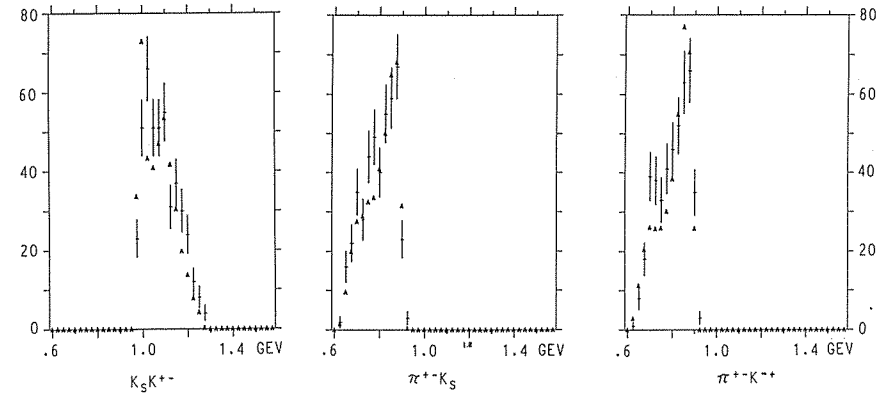

EFFECTIVE MASS DISTRIBUTION

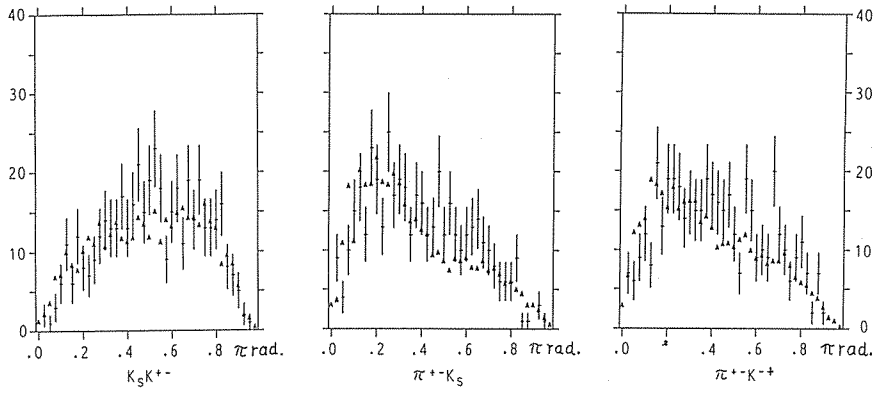

θ DISTRIBUTION

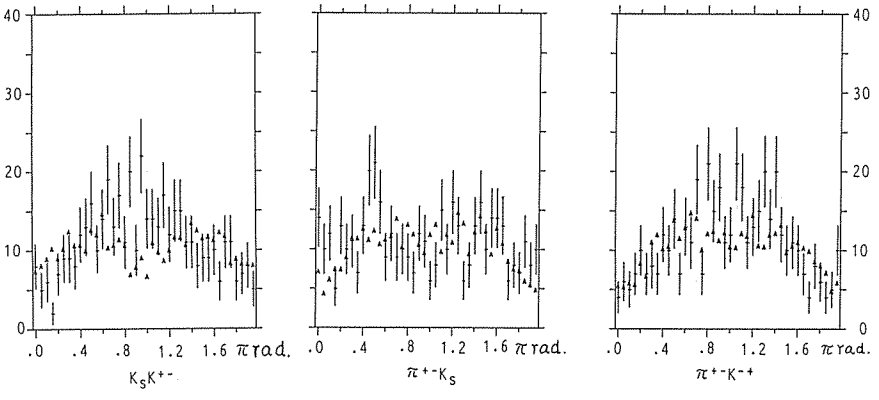

α DISTRIBUTION

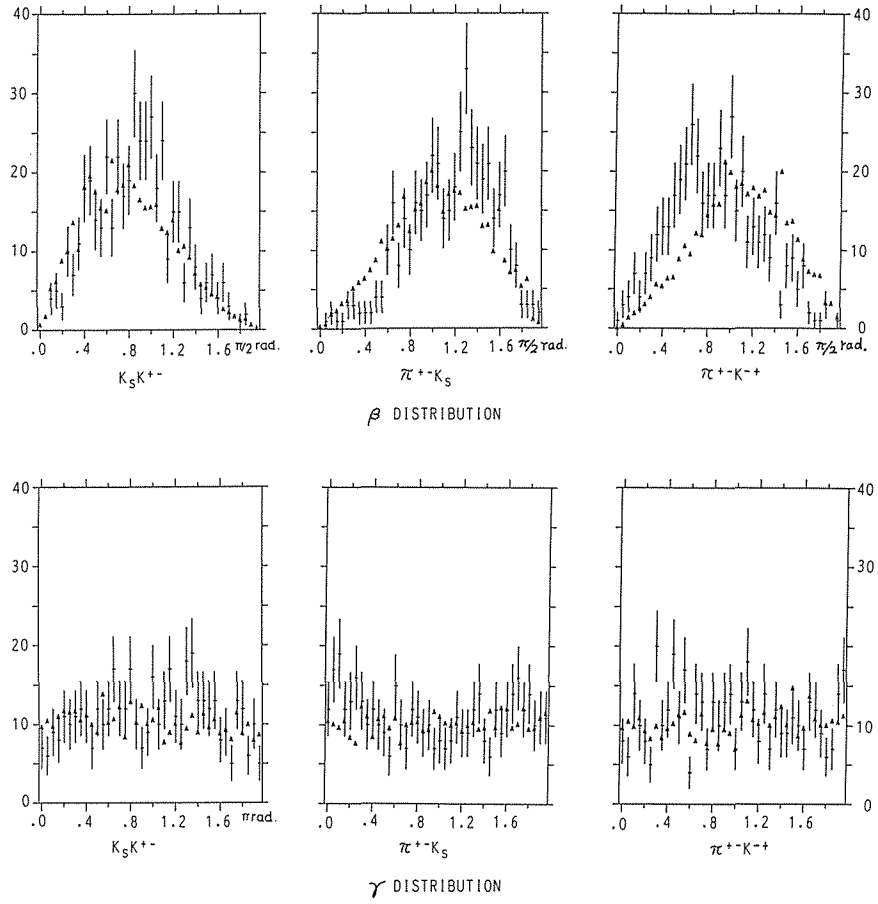

Figure 18 Distribution of five kinematical variables, α, β, γ, ω and θ. The results of Monte Carlo simulation using the fitted amplitudes at $m_{K\bar{K}\pi}=1.42$ GeV are plotted by A. The data in this mass range($1.39<m_{K\bar{K}\pi}<1.45$ GeV) are plotted by crosses, for comparison.

mass region is limited below 1.6 GeV.

The observation of the isoscalar of 1^{++} nonet at a mass of 1.53 GeV in the $K^-p\to(K^\pm K_s\pi^\mp)\Lambda$ reaction was reported by Gavillet et al.[32] It is called D' and observed in the peripheral production. The enhancement in the $0-+K^*K$ wave is also peripheral but the spin parity is different with D'.

The increase of the $1--K^*KP0-$ wave up to 1.6 GeV region seemed to be mainly due to the production of ω or ϕ' which are the isoscalar vector meson state. The increase of the wave may relate with the decrease of the $0-+K^*K$ wave at high mass region which makes the 1.52 GeV peak like a resonance.

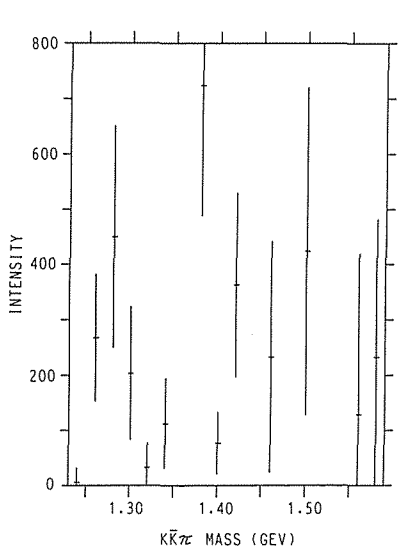

19a $1++\delta\pi P0+$ wave

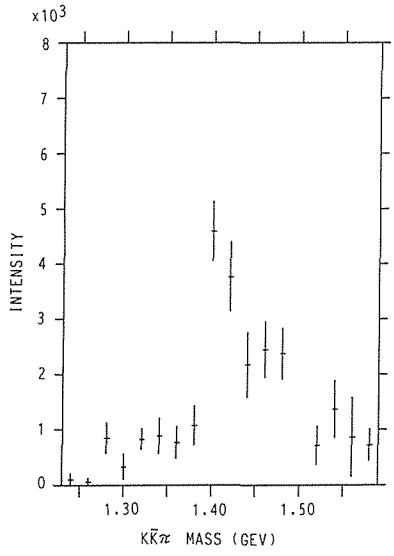

19b $0-+\delta\pi S0+$ wave

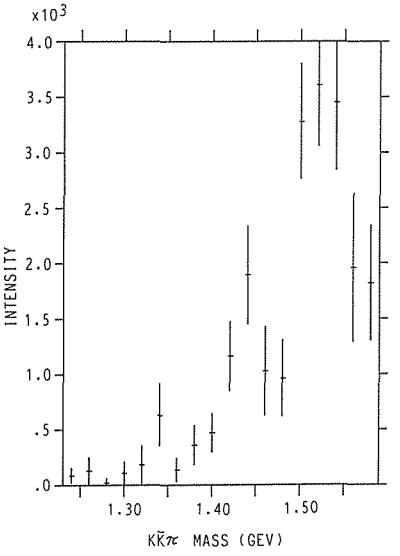

19c $0-+K^{\ddagger}KP0+$ wave

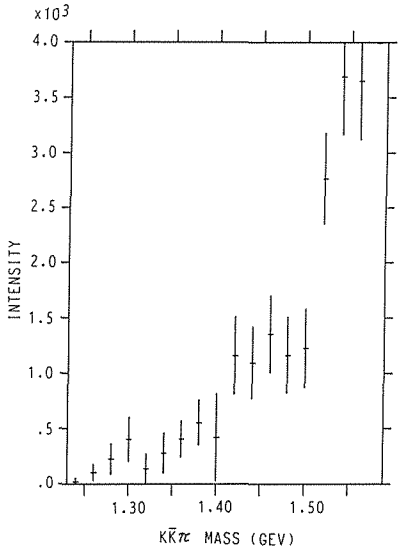

19d $1--K^{K}P0-$ wave

Figure 19 Intensities of the significant waves corrected with the acceptance. The notation is described in the text.

6. Conclusions

4000 samples of $K^{\pm}K_s\pi^{\mp}$ have been successfully collected. The K_s mesons were tagged by the vertex topology and the effective mass calculation in present analysis. The charged kaon and pions are clearly distinguished by the TOF method. The recoil neutron was identified clearly by the missing mass calculation. The selection of the

events from the background of four charged pions has been satisfactorily performed. Two enhancements around 1.28 GeV and 1.42 GeV in the $K^{\pm}K_s\pi^{\mp}$ effective mass distribution have been observed. The fitted mass and width with the Breit-Wigner function at 1.42 GeV were 1.424 ± 0.006 GeV and 35 ± 6 MeV, respectively. Those at the 1.28 GeV region are also found to be 1.280 ± 0.006 GeV(W) and 15 ± 5 MeV(Γ). The so called δ cut enhanced these peaks. This indicates that these states decay mainly through the $\delta\pi$ intermediate state. However, the K^* cut also enhances the peak around 1.42 GeV. The Dalitz plot in the mass region of the $K\overline{K}\pi$ system around 1.42 GeV shows the K^* band and a considerable amount of events around the δ line. The mass region near 1.5 GeV is dominated by the K^*K production rather than the three body phase space distribution.

The partial wave analysis has been performed to study the intermediate state, spin and parity especially at the 1.42 GeV peak. The $1++\delta\pi P0+$ wave has a peak at 1.28 GeV which corresponds to D(1280). The $0-+\delta\pi S0+$ wave showed a prominent mass structure around 1.42 GeV. The enhancement at 1.42 GeV in the effective mass distribution and that in the $0-+\delta\pi S0+$ wave correspond to the E(1420) meson. Our data favor the 0^{-+} assignment for the E(1420) meson. This state decays mainly into $\delta\pi$ and seems to have rather small decay width into $K^*\overline{K}+\overline{K}^*K$.

The mass region around 1.52 GeV is dominated by the $0-+K^*KP0+$ wave. However, it is not clear whether nonresonant background causes such effect or there exists another pseudoscalar meson.

Acknowledgements

I would like to express my gratitude to Prof. K. Takamatu, Dr. T. Tsuru, Dr. T. Inagaki and Prof. T. Sato of KEK who gave me both guidance and help with all aspects of the experiment.

I would like to express my appreciation to the members of our collaboration who contributed to the success of this experiment: Prof.T. Nakamura, Dr. N. Tamura, Dr. K. Imai, and Dr. Y. Inagaki of Kyoto University and Dr. A. Itano of National Institute of Radiogical Sciences, Prof. A. Murakami and Dr. S. Kobayashi of Saga University, Prof. H. Okuno and Dr. K. Maruyama of INS of Tokyo University, Prof. A. Sasaki of Akita University, Prof. A. Ando of RCNP of Osaka University, Dr. S. Inaba and Mr. Yasu of KEK.

My thanks also goes to my fellow research workers Dr. J. Shirai of KEK who led me from the early stage of the experiment and Dr. Ohmi of Tsukuba University who taught me the technique of the partial wave analysis.

My physics advisor, Prof. K. Miyake gave me both support and encouregement throughout the experiment.

This work would not be completed without the contribution of those people. My thanks also goes to all the staff of KEK whose continuous effort has made this experiment possible.

Reference

1) R. L. Jaffe and K. Johnson, Phys. Lett. **60B**, 201 (1976)
J. J. Coyne, P. M. Fishbane and S. Meshikov, Phy. Lett. **91B**, 259 (1980)
J. F. Donoghue, K. Johnson and B . A. Li, Phys. Lett. **99B**, 416 (1981)
G. Bhanot, Phys. Lett. **101B**, 95 (1981)
J. M. Cornwall and A. Soni, Phys. Lett. **120B**, 431 (1983)
2) T. Appelquist and H. D. Politzer, Phys. Rev. **D12**, 1404 (1975)
M. S. Chanowitz, Phys. Rev.**D12**, 918 (1975)
3) H. J. Lipkin, ANL-HEP-PR-81-23, June, 1981
H. J. Lipkin, Phys. Lett. **109B**, 326 (1982)
4) D. Robson, Nucl. Phys. **B130**, 328 (1977)
5) R. Armenteros et al., Proceedings of the Siena International Conference of Elementary Particles Vol. 1,287 (1963)
6) P. Billon et al., Nuovo Cim. **A50**,393 (1967)
7) O. I. Dahl et al., Phys. Rev. **163**, 1377 (1967)
8) B. Lorstad et al., Nucl. Phys. **B14**, 63 (1969)
9) R. Nacasch et al., Nucl. Phys. **B135**, 203 (1978)
10) C. Dionisi et al., Nucl. Phys. **B169**, 1, (1980)
11) D. L. Scharre et al., Phys. Lett. **97B**, 329 (1980)
12) K. Ishikawa, Phys. Rev. Lett. **46**, 978 (1981)
13) M. Chanowitz, Phys. Rev. Lett. **46**, 981 (1981)
14) C. Edwards et al.,Phys. Rev. Lett. **49**, 259 (1982)
15) C. Edwards et al., Phys. Rev. Lett. **51**, 859 (1983)
16) J. D. Richman Ph. D. Thesis, Califolnia Institute of Technology (1985)
17) T. A. Armstrong et al., Phys. Lett. **146B**, 273 (1984)
18) S. U. Chung et al., Phys.Rev. Lett. **55**, 779 (1985)
19) N. R. Stanton et al., Phys. Rev. Lett. **42**, 346 (1979)
20) A. Ando et al., Phys. Rev. Lett. **57**, 1296 (1986)
21) J. Shirai, Memoirs of the Fuculty of Science, Kyoto University, Series of Physics, Astorophysics, Geophysics and Chemistry, Vol. **37**, No. 3, (1986)
22) T. Inagaki and R. Takashima, Nucl. Instrum. Meth. **201**, 511 (1982)
23) T. Tanimori et al., Nucl. Instrum. Meth. **216**, 57 (1983)
24) K. Ikeno et al., Nucl. Instrum. Meth. **225**, 347 (1984)
25) H. Wind, Nucl. Instrum. Meth. **115**, 431(1974)
26) D. J. Herndon, P.Sording and R. J. Cashmore, Phys.Rev. **D11**, 3165 (1975)
27) J. M. Blatt and V. F. Weiskopf, Theoretical Nuclear Physics, J.Willey and Sons, NY (1966) p 361
28) J. D. Hansen et al., Nucl. Phys. **B81**, 403 (1974)
29) D. J. Herndon et al., Phys. Rev. **D11**, 3183 (1975)
30) J. A. Dankowych Ph. D. Thesis University of Tronto (1980)
We would like to thank Dr. J. A.Dankowych for sending us a copy of the isobar model program.
31) P. E. Eberhard, W. O. Koellner, Comp. Phys. Comm. **3**, 296 (1972)
32) Ph. Gavillet et al., Z. Phys. **C16**, 119 (1982)